

Clean Images are Hard to Reblur: A New Clue for Deblurring

Seungjun Nah

Sanghyun Son

Jaerin Lee

Kyoung Mu Lee

ASRI, Department of ECE, Seoul National University, Korea

seungjun.nah@gmail.com, {thstkgus35, ironjr, kyoungmu}@snu.ac.kr

Abstract

The goal of dynamic scene deblurring is to remove the motion blur present in a given image. Most learning-based approaches implement their solutions by minimizing the $L1$ or $L2$ distance between the output and reference sharp image. Recent attempts improve the perceptual quality of the deblurred image by using features learned from visual recognition tasks. However, those features are originally designed to capture the high-level contexts rather than the low-level structures of the given image, such as blurriness. We propose a novel low-level perceptual loss to make image sharper. To better focus on image blurriness, we train a reblurring module amplifying the unremoved motion blur. Motivated that a well-deblurred clean image should contain zero-magnitude motion blur that is hard to be amplified, we design two types of reblurring loss functions. The supervised reblurring loss at training stage compares the amplified blur between the deblurred image and the reference sharp image. The self-supervised reblurring loss at inference stage inspects if the deblurred image still contains noticeable blur to be amplified. Our experimental results demonstrate the proposed reblurring losses improve the perceptual quality of the deblurred images in terms of NIQE and LPIPS scores as well as visual sharpness.

1. Introduction

Dynamic scene deblurring aims to remove unwanted motion blur from an image and recover the latent sharp image. Blind image deblurring is a challenging ill-posed problem as both the locally-varying blur kernel and the latent image have to be found from large solution space. Traditional optimization-based approaches [11, 46, 14, 15] tried to relieve the ill-posedness by designing priors that reflect the statistical properties of desired solutions. With \mathbf{B} , \mathbf{L} as vectorized blurry and the latent images and the large kernel matrix \mathbf{K} , a typical energy formulation is

$$\arg \min_{K,L} \|\mathbf{B} - \mathbf{KL}\| + E_{\text{prior}}(\mathbf{K}, \mathbf{L}). \quad (1)$$



Figure 1: **Comparison of the deblurred images and their reblurred counterparts.** For each image, we visualize the remaining blur kernel [7] at the center pixel visualized on the right bottom side. **Upper:** The kernels from the previous methods implicate the direction of the original blur. **Lower:** When the proposed reblurring module is applied, our result does not lose sharpness as we reconstruct the output that is hard to be reblurred.

Instead of using such handcrafted knowledge, recent deep learning methods take advantage of learning from large-scale datasets [27, 38, 30, 26, 36]. Usually, the learning is enabled by minimizing Euclidean distance loss, e.g., $L1$ or $L2$, to maximize PSNR between the deblurred and the reference sharp images. With the advent of modern CNN architectures, state-of-the-art deblurring networks [27, 42, 8, 48, 32] have been developed toward better model capacity and deblurring accuracy. Still, most methods tend to suffer from blurry predictions due to the inherent limitation [20, 23] of PSNR-oriented solutions for ill-posed problems. To complement the conventional learning objectives, several attempts such as the perceptual [13] and the adversarial loss [20, 27, 17] have been made to improve the visual quality and the sharpness of the model output. Nevertheless, the previous perceptual losses may not be optimal for blur removal as the low-level structural properties such as blurriness are not explicitly considered in their formulations. Rather, they originate from features learned for high-level tasks such as image classification and real/fake image

discrimination. As illustrated in Figure 1, results from the existing deblurring methods are not as sharp as the ground-truth example but are still blurry to a degree. Despite the reduced strength of blur in the deblurred images, we still observe the directional motion information remaining.

The observation tells that applying the VGG and the adversarial loss together [18] is not sufficient to obtain perceptually pleasing and sharp images across different architectures [43, 18]. By finding the inherent limitation of the previous loss terms, we conjecture that eliminating the motion cues remaining in the deblurred images could play an essential role in generating sharp and clean images. Starting from the motivation, we introduce the concept of *reblurring* which amplifies the unremoved blur in the given image. An ideally deblurred image should be sharp enough so that no noticeable blur can be found from it to be amplified, i.e., clean images are hard to reblur. In contrast, it is easier to predict the original shape of blur by recognizing the remaining blur kernel if the motion blur is not sufficiently removed. We propose to use the difference as the new optimization objective, *reblurring loss* for image deblurring problem.

The reblurring loss is realized by jointly training a deblurring module and the paired reblurring module. From a deblurred output, the reblurring module tries to make the reblurred image as close to the original blurry image. By using the property that the reblurred results should vary by the degree of input blur to be amplified, we construct two types of loss functions. During the joint training, *supervised reblurring loss* compares the amplified blurs between the deblurred and the sharp image. Complementing the L1 intensity loss, the supervised reblurring loss guides the deblurring module to focus on and eliminate the remaining blur information. While the training method being similar to the adversarial training of GANs [10], the purposes and effects of the adversary are different. Our reblurring loss concentrates on the image blurriness regardless of the image realism in the training process. Furthermore, we apply *self-supervised reblurring loss* at test-time so that the deblurred image would be infeasible to be reblurred as sufficiently sharp image would. The self-supervised reblurring loss lets the deblurring module to adaptively optimize to each input without ground truth.

The reblurring loss functions provide additional optimization directives to the deblurring module and can be generally applied to any learning-based methods. With the proposed approach, sharper images can be obtained without modifying the structure of the deblurring module.

We summarize our contributions as follows:

- Based on the observation that clean images are hard to reblur, we propose novel loss functions for image deblurring. Our reblurring loss reflects the preference for sharper images and contributes to visually pleasing deblurring results.

- At test-time, the reblurring loss can be implemented without a ground-truth image. We perform test-time adaptive inference via self-supervised optimization to each input.
- Our method is generally applicable to any learning-based methods and jointly with other loss terms. Experiments show that the concept of reblurring loss consistently contributes to achieving state-of-the-art visual sharpness as well as LPIPS and NIQE across different model architectures.

2. Related Works

Image Deblurring. In the classic energy optimization framework, the energy is formulated by the likelihood and the prior term. Due to the large solution space of the ill-posed dynamic scene deblurring problem, prior terms have been the essential element in alleviating the optimization ambiguity by encoding the preference on the solutions. Sophisticated prior terms were carefully designed with human knowledge on natural image statistics [21, 7, 11, 46, 41, 47, 14, 15, 31]. In the recent work of Li *et al.* [22], learned prior, which is derived from a classifier discriminating blurry and clean images, was also shown to be effective. Deep priors were also used for image deconvolution problems [33, 28].

On the other hand, deep learning methods have benefited from learning on large-scale datasets. The datasets consisting of realistic blur [27, 38, 30, 26, 8, 12, 36] align the temporal center of the blurry and the sharp image pairs with high-speed cameras. Learning from such temporally aligned datasets relieves the ill-posedness of deblurring compared with the large solution space in the energy optimization framework. Thus, more attention has been paid to designing CNN architectures and datasets than the loss or solution preference.

In the early work, the alternating kernel and image estimation processes [7] are implemented with CNNs [35]. In [40, 9], the spatially varying blur kernels are estimated by assuming locally linear blur followed by non-blind deconvolution with them. Later, end-to-end learning without explicit kernel estimation became prevalent. Motivated from the coarse-to-fine approach, multi-scale CNN was proposed in [27] to expand the receptive field efficiently. Several studies have proposed scale-recurrent architectures [43, 8] that share parameters across the scales. On the other hand, [49, 39] sequentially stacked network modules. Recently, [32] proposed a multi-temporal model that deblurs an image recursively. To handle spatially varying blur kernels efficiently, spatially non-uniform operations were embedded [50, 48] in the neural networks.

Perceptual Image Restoration. Conventional image restoration methods mainly optimize L1 or L2 objectives to achieve higher PSNR. However, such approaches suffer from blurry and over-smoothed outputs [13, 52, 23]. The

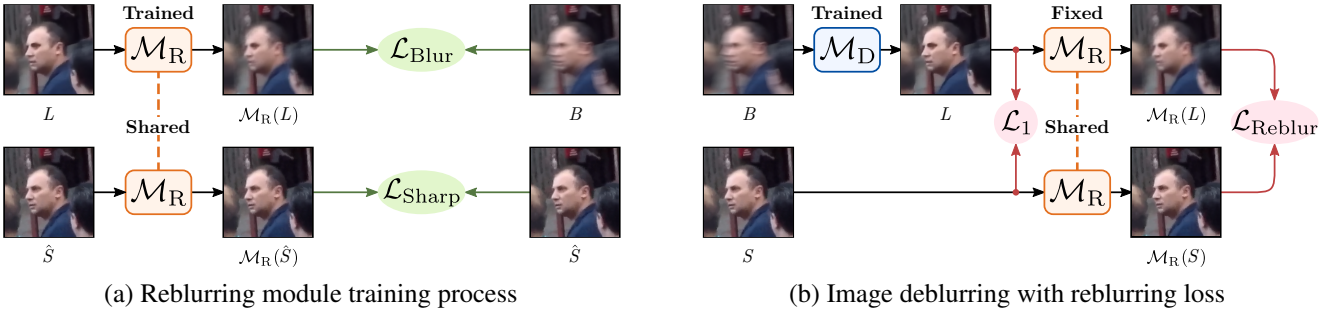


Figure 2: **Overviews of the proposed reblurring and deblurring framework.**

primary reason is that the learned models predict an average of all possible solutions under the ill-posedness [20]. To deal with the issue, several studies utilize deep features of the pretrained VGG [37] network that are more related to human perception [13, 20, 52]. Then, the following methods can produce perceptually better results by minimizing the distance of output and ground-truth images in the feature domain. Recent methods further introduce adversarial training [10] so that outputs of the restoration models be indistinguishable from real samples [27, 29, 17, 18].

Nevertheless, an inherent limitation of existing perceptual objectives is that they are not task-specialized for image restoration. For example, the VGG features [37] are learned for high-level visual recognition [34] while adversarial loss [10] only contributes to reconstruct realistic images without considering the existence of motion blur. Therefore, blindly optimizing those terms may not yield an optimal solution in terms of image deblurring. In practice, we observed that those objectives still tend to leave blur footprints unremoved, making it possible to estimate the original blur. Our reblurring loss is explicitly designed to improve the perceptual quality of deblurred images by reducing remaining blurriness and thus more suitable for the deblurring task.

Image Blurring. As an image could be blurred in various directions and strength, image blurring is another ill-posed problem. Thus intrinsic [1] or extrinsic [6, 5] information is often incorporated. In the case of a non-ideally sharp image, Bae *et al.* [1] detected the small local blur kernel in the image to magnify the defocus blur for the bokeh effect. On the other hand, [6] estimated the kernel by computing the optical flow from the neighboring video frames. In a similar sense, [5] used multiple video frames to synthesize blur. Without such blur or motion cue, there could be infinitely many types of plausible blur applicable to an image. Thus, [51] used a generative model to synthesize many realistic blurry images. Contrary to the above approaches, [2] deliberately blurred an already blurry image in many ways to find the local blur kernel. Our image reblurring concept is similar to [1] in the sense that intrinsic cue in an image is

#ResBlocks	4	8	16	32
Deblur PSNR wrt sharp GT	28.17	29.67	30.78	31.48
Reblur PSNR wrt blur GT	34.29	32.66	31.90	31.48

Table 1: **Deblurring and reblurring PSNR (dB) by deblurring model capacity.** Both tasks are trained independently with L1 loss on the GOPRO [27] dataset. We note that #ResBlocks varies for the deblur network only.

used to amplify blur. Nonetheless, our main goal is to use reblurring to provide a guide to deblurring model so that such blur cues would be removed.

3. Proposed Method

In this section, we describe a detailed concept of image reblurring and how the reblurring operation can be learned. The proposed reblurring loss can support the deblurring modules to reconstruct perceptually favorable and sharp outputs. At training and testing stages, we formulate the reblurring loss in supervised and self-supervised manner. For simplicity, we refer to the blurry, the deblurred, and the sharp image as B , L , and S , respectively.

3.1. Clean Images are Hard to Reblur

As shown in Figure 1, outputs from the existing deblurring methods still contain undesired motion trajectories that are not completely removed from the input. Ideally, a well-deblurred image should not contain any motion cues making reblurring to be infeasible. To validate our motivation that clean images are hard to reblur, we first build a reblurring module \mathcal{M}_R which amplifies the remaining blur from L . The module is trained with the following blur reconstruction loss \mathcal{L}_{Blur} so that it would learn the inverse operation of deblurring.

$$\mathcal{L}_{Blur} = \|\mathcal{M}_R(L) - B\|. \quad (2)$$

We apply \mathcal{M}_R to the deblurred images from deblurring modules of varying capacities. Table 1 shows that the higher the deblurring PSNR, the lower the reblurring PSNR becomes. It demonstrates the better deblurred images are harder to reblur, justifying our motivation.

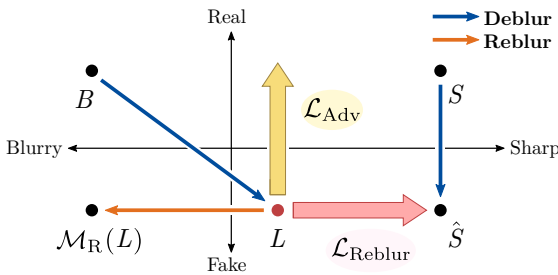


Figure 3: **Image deblurring and reblurring illustrated from the perspective of sharpness and realism.** Training our modules with $\mathcal{L}_{\text{Reblur}}$ improves image sharpness without considering the image realism. The image realism can be optionally handled by adversarial loss \mathcal{L}_{Adv} .

In contrast to the non-ideally deblurred images, \mathcal{M}_R is not able to generate a motion blur from a sharp image S . For a high-quality clean image, \mathcal{M}_R should preserve the sharpness. However, optimizing the blur reconstruction loss $\mathcal{L}_{\text{Blur}}$ with S may fall into learning the pixel average of all blur trajectories in the training dataset. In such a case, \mathcal{M}_R will apply a radial blur without considering the input variety. To let the blur domain of \mathcal{M}_R be confined to the motion-incurred blur, we use sharp images to penalize such undesired operation. Specifically, we introduce a network-generated sharp image \hat{S} obtained by feeding a real sharp image S to the deblurring module \mathcal{M}_D , as $\hat{S} = \mathcal{M}_D(S)$. We define sharpness preservation loss $\mathcal{L}_{\text{Sharp}}$ as follows:

$$\mathcal{L}_{\text{Sharp}} = \|\mathcal{M}_R(\hat{S}) - \hat{S}\|. \quad (3)$$

We use pseudo-sharp image \hat{S} instead of a real image S to make our reblurring module focus on image sharpness and blurriness rather than image realism. While \hat{S} and L only differ by the sharpness, S and L also vary by their realism.

Combining two loss terms together, we train the reblurring module \mathcal{M}_R by optimizing the joint loss \mathcal{L}_R :

$$\mathcal{L}_R = \mathcal{L}_{\text{Blur}} + \mathcal{L}_{\text{Sharp}}. \quad (4)$$

As zero-magnitude blur should remain unaltered from \mathcal{M}_R , the sharpness preservation loss can be considered a special case of the blur reconstruction loss. Figure 2a illustrates the way our reblurring module is trained from \mathcal{L}_R .

3.2. Supervision from Reblurring Loss

The blurriness of images can be easily compared by amplifying the blur. Thus, we propose a new optimization objective by processing the deblurred and the sharp image with the proposed reblurring model \mathcal{M}_R . To suppress remaining blur in the output L of the deblurring CNN \mathcal{M}_D , our reblurring loss $\mathcal{L}_{\text{Reblur}}$ for image deblurring is defined as follows:

$$\mathcal{L}_{\text{Reblur}} = \|\mathcal{M}_R(L) - \mathcal{M}_R(S)\|. \quad (5)$$

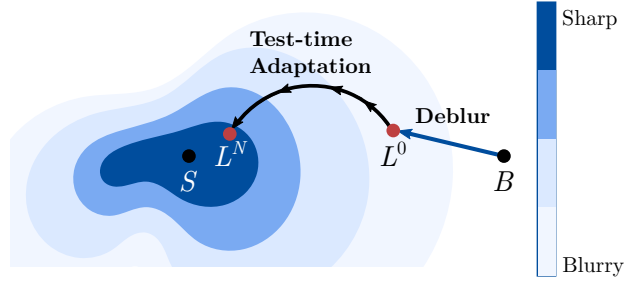


Figure 4: **The proposed self-supervised test-time adaptation.** We repetitively find the latent image that reblurs to the current deblurred image.

Unlike the sharpness preservation term in (3), we do not use the pseudo-sharp image \hat{S} in our reblurring loss (5). As the quality of the pseudo-sharp image \hat{S} depends on the state of deblurring module \mathcal{M}_D , using \hat{S} may make training unstable and difficult to optimize, especially at the early stage. Thus we use a real sharp image S to stabilize the training. Nevertheless, as \mathcal{M}_R is trained to focus on the sharpness from (4), so does the reblurring loss $\mathcal{L}_{\text{Reblur}}$.

Using our reblurring loss in (5), the deblurring module \mathcal{M}_D is trained to minimize the following objective \mathcal{L}_D :

$$\mathcal{L}_D = \mathcal{L}_1 + \lambda \mathcal{L}_{\text{Reblur}}, \quad (6)$$

where \mathcal{L}_1 is a conventional L1 loss, and the hyperparameter λ is empirically set to 1. Figure 2b shows how the deblurring model is trained with our proposed reblurring loss.

For each training iterations, we alternately optimize two modules \mathcal{M}_D and \mathcal{M}_R by \mathcal{L}_D and \mathcal{L}_R , respectively. While such a strategy may look similar to the adversarial training [10], the optimization objectives are different. As the neural networks are well known to easily discriminate real and fake images [44], the realism could serve as a more salient feature than image blurriness. Thus, adversarial loss may overlook image blurriness as L and S can already be discriminated by realism difference. On the other hand, our reblurring loss is explicitly designed to prefer sharp images regardless of realism. Figure 3 conceptually compares the actual role of the proposed reblurring loss $\mathcal{L}_{\text{Reblur}}$ and the existing adversarial loss \mathcal{L}_{Adv} .

3.3. Test-time Adaptation by Self-Supervision

Supervised learning methods have the fixed model weights at testing time as the training with ground truth is no longer available. Every image is treated equally regardless of the scene content and the blur difficulty at test time. In contrast, providing self-supervised loss can make a model adapt to each test input, improving the generalization ability. Thus, we use the proposed reblurring operation to enable a novel self-supervised optimization without the need for ground truth.

During the training of \mathcal{M}_D , \mathcal{M}_R delivers supervision from the reference by (5). With the learned reblurring op-

Algorithm 1 Optimization process in test-time adaptation

```

1: procedure TEST-TIME ADAPTATION( $B, \mathcal{M}_D, \mathcal{M}_R$ )
2:   Test-time learning rate  $\mu \leftarrow 3 \times 10^{-6}$ .
3:    $\theta_D \leftarrow$  Weights of  $\mathcal{M}_D$ .
4:    $L^0 = \mathcal{M}_D(B)$ .
5:   for  $i = 0 \dots N - 1$  do
6:      $L_*^i = \mathcal{M}_D(B)$ .
7:      $\mathcal{L}_{\text{reblur}}^{\text{self}} = \|\mathcal{M}_R(\mathcal{M}_D(B)) - L_*^i\|$ .
8:     Update  $\theta_D$  by  $\nabla_{\theta_D} \mathcal{L}_{\text{reblur}}^{\text{self}}$  and  $\mu$ .
9:      $L^N = \mathcal{M}_D(B)$ .
10:     $L_{\text{Adapted}}^N = \text{histogram\_matching}(L^N, L_*^0)$ 
11:   return  $L_{\text{Adapted}}^N$ 

```

eration, we can further exploit the deblurred image L is in high-quality in terms of shaprness without reference data. If L gets blurred by passing to \mathcal{M}_R , we can consider it to be insufficiently deblurred as we have discussed in Figure 1. A clean image should remain as itself due to the sharpness preservation loss, $\mathcal{L}_{\text{Sharp}}$. Thus, we construct the self-supervised reblurring loss that could serve as a prior term encoding the preference on sharp images.

$$\mathcal{L}_{\text{Reblur}}^{\text{self}} = \|\mathcal{M}_R(L) - L_*\|, \quad (7)$$

where L_* denotes the image with the same value as L but the gradient does not backpropagate in the optimization process. We minimize $\mathcal{L}_{\text{Reblur}}^{\text{self}}$ for each test data to obtain the sharper image. Allowing gradient to flow through L_* can let L to fall into undesired local minima where both the L and $\mathcal{M}_R(L)$ are blurry. Since $\mathcal{L}_{\text{Reblur}}^{\text{self}}$ only considers the sharpness of an image, we keep the color consistency by matching the color histogram between the test-time adapted image and the initially deblurred image. The detailed process of test-time adaptation strategy is described in Algorithm 1 and conceptually illustrated in Figure 4.

4. Experiments

We demonstrate the effectiveness of our reblurring loss by applying it to multiple model architectures. We show the experimental results with a baseline residual U-Net and the state-of-the-art image deblurring models, the sRGB version of SRN [43] and DHN, our modified version of DM-PHN [49]. For the reblurring module, we use simple residual networks with 1 or 2 ResBlock(s) with 5×5 convolution kernels. The training and evaluation were done with the widely used GOPRO [27] and REDS [26] datasets. The GOPRO dataset consists of 2103 training and 1111 test images with various dynamic motion blur. Similarly, the REDS dataset has 24000 training and 3000 validation data publicly available. On each dataset, every experiment was done under the same training environment. We mainly compare LPIPS [52] and NIQE [25] perceptual metrics. For

Method	LPIPS \downarrow	NIQE \downarrow	PSNR \uparrow	SSIM \uparrow
U-Net (\mathcal{L}_1 only)	0.1635	5.996	29.66	0.8874
	+ $\mathcal{L}_{\text{Reblur, n1}}$	0.1365	5.629	0.8869
	+ $\mathcal{L}_{\text{Reblur, n2}}$	0.1238	5.124	0.8824
SRN (\mathcal{L}_1 only)	0.1246	5.252	30.62	0.9078
	+ $\mathcal{L}_{\text{Reblur, n1}}$	0.1140	5.136	0.9104
	+ $\mathcal{L}_{\text{Reblur, n2}}$	0.1037	4.887	0.9074
DHN (\mathcal{L}_1 only)	0.1179	5.490	31.53	0.9207
	+ $\mathcal{L}_{\text{Reblur, n1}}$	0.0975	5.472	0.9217
	+ $\mathcal{L}_{\text{Reblur, n2}}$	0.0837	5.076	0.9177

Table 2: **Perceptual metric improvements from the reblurring loss on GOPRO [27] dataset.** The reblurring loss consistently improves LPIPS and NIQE over standard \mathcal{L}_1 loss.

Method	LPIPS \downarrow	NIQE \downarrow	PSNR \uparrow	SSIM \uparrow
U-Net (\mathcal{L}_1 only)	0.1486	3.649	30.80	0.8772
	+ $\mathcal{L}_{\text{Reblur, n1}}$	0.1435	3.487	0.8776
	+ $\mathcal{L}_{\text{Reblur, n2}}$	0.1252	2.918	0.8717
SRN (\mathcal{L}_1 only)	0.1148	3.392	31.89	0.8999
	+ $\mathcal{L}_{\text{Reblur, n1}}$	0.1071	3.305	0.9044
	+ $\mathcal{L}_{\text{Reblur, n2}}$	0.0947	2.875	0.9026
DHN (\mathcal{L}_1 only)	0.0942	3.288	32.65	0.9152
	+ $\mathcal{L}_{\text{Reblur, n1}}$	0.0931	3.248	0.9143
	+ $\mathcal{L}_{\text{Reblur, n2}}$	0.0805	2.830	0.9122

Table 3: **Quantitative comparison on REDS [26] dataset by loss function.** The reblurring loss improves LPIPS and NIQE over standard \mathcal{L}_1 loss.

more detailed implementation details, please refer to the supplementary material.

4.1. Effect of Reblurring Loss

We implement the reblurring loss in varying degrees of emphasis on sharpness by controlling the reblurring module capacity. For a more balanced quality between PSNR and perceptual sharpness, we use 1 ResBlock for \mathcal{M}_R . To put more weight on the perceptual quality, we allocate a larger capacity on \mathcal{M}_R by using 2 ResBlocks. For notation simplicity, we denote the reblurring loss with k ResBlock(s) in the reblurring module as $\mathcal{L}_{\text{Reblur, n}k}$.

Table 2 and 3 each shows how the deblurring performance varies depending on the training loss functions. With $\mathcal{L}_{\text{Reblur, n}1}$, LPIPS and NIQE improves to a moderate degree while PSNR and SSIM metrics remain at a similar level. Meanwhile, $\mathcal{L}_{\text{Reblur, n}1}$ more aggressively optimizes the perceptual metrics. The perceptual metric improvements are consistently witnessed with different architectures on both the GOPRO and the REDS dataset.

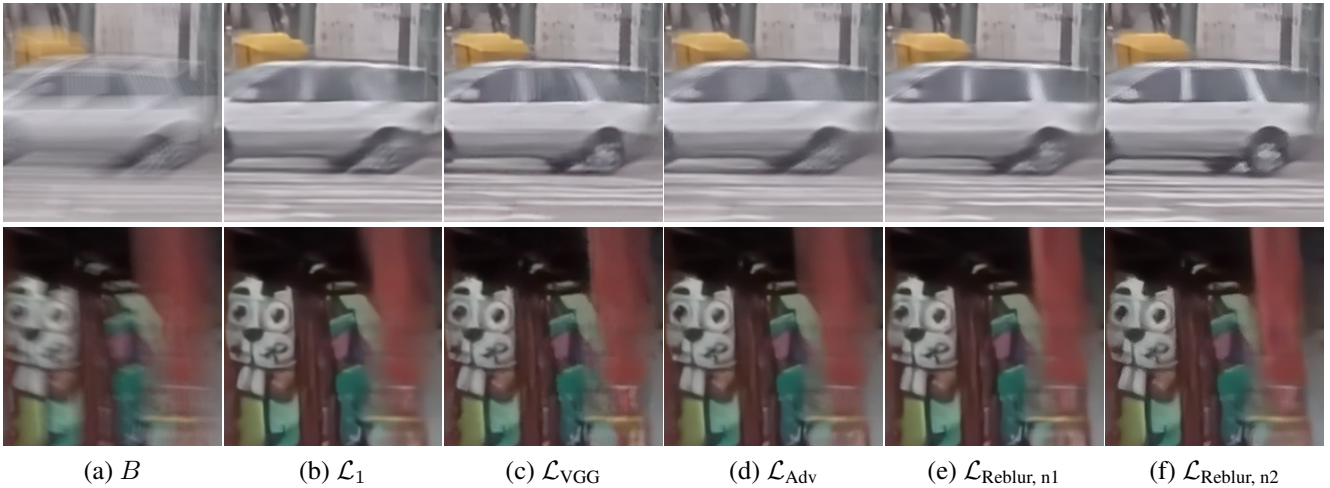


Figure 5: **Visual comparison of deblurred results by training loss function on GOPRO dataset. Upper: SRN, Lower: U-Net.**

Method	LPIPS _↓	NIQE _↓	PSNR [↑]	SSIM [↑]
U-Net ($\mathcal{L}_{\text{Blur}}$ only)	0.1301	5.132	29.47	0.8839
$+ \mathcal{L}_{\text{Sharp}}$ with S	0.1410	5.307	29.15	0.8694
$+ \mathcal{L}_{\text{Sharp}}$ with \hat{S}	0.1238	5.124	29.44	0.8824

Table 4: **The effect of the sharpness preservation in training our reblurring module measured on GOPRO [27] dataset.** In (3), using the pseudo-sharp image \hat{S} instead of the real one S leads to better deblurring performance. We note that the reblurring module is constructed using 2 ResBlocks.

4.2. Effect of Sharpness Preservation Loss

In training \mathcal{M}_R , we used both the blur reconstruction loss $\mathcal{L}_{\text{Blur}}$ and the sharpness preservation loss $\mathcal{L}_{\text{Sharp}}$. The latter term $\mathcal{L}_{\text{Sharp}}$ plays an essential role in concentrating only on the motion-driven blur in the given image and keeping sharp image sharp. Table 4 presents the performance gains from using $\mathcal{L}_{\text{Sharp}}$ jointly with $\mathcal{L}_{\text{Blur}}$ in terms of the perceptual quality.

Table 4 also justifies the effectiveness of the pseudo-sharp image \hat{S} in sharpness preservation. We found the using with S for $\mathcal{L}_{\text{Sharp}}$ in addition to $\mathcal{L}_{\text{Blur}}$ causes less stable training than using \hat{S} . Using the pseudo-sharp image confines the input distribution of \mathcal{M}_R to the output domain of \mathcal{M}_D . While the real sharp data S differ from the deblurred image L in terms of realness, the pseudo-sharp image \hat{S} only differs by the sharpness. Thus the reblurring module can focus on the image sharpness without being distracted by other unintended properties. Furthermore, it leads the two loss terms $\mathcal{L}_{\text{Blur}}$ and $\mathcal{L}_{\text{Sharp}}$ to reside under the same objective, amplifying any noticeable blur and keeping sharpness when blur is not found.

Method	LPIPS _↓	NIQE _↓	PSNR [↑]	SSIM [↑]
SRN (\mathcal{L}_1)	0.1246	5.252	30.62	0.9078
$+ 0.001 \mathcal{L}_{\text{Adv}}$	0.1141	4.960	30.53	0.9068
$+ 0.3 \mathcal{L}_{\text{VGG}}$	0.1037	4.945	30.60	0.9074
$+ \mathcal{L}_{\text{Reblur, n2}}$	0.1037	4.887	30.57	0.9074

Table 5: **Comparison of reblurring loss and other perceptual losses on GOPRO [27] dataset applied to SRN.**

4.3. Comparison with Other Perceptual Losses

The reblurring loss provides a conceptually different learning objectives from the adversarial and the perceptual losses and is designed to focus on the motion blur. Table 5 compares the effectiveness of $\mathcal{L}_{\text{Reblur}}$ with adversarial loss \mathcal{L}_{Adv} , and the VGG perceptual loss [13] by applying them to SRN [43] on GOPRO dataset. While our method provides quantitatively better perceptual scores, the different perceptual losses are oriented to varying goals and are not in essentially competing relation. They do not necessarily conflict with each other and can be jointly applied in training to catch the perceptual quality in varying aspects.

4.4. Effect of Test-time Adaptation

We conduct test-time adaptation with the proposed self-supervised reblurring loss, $\mathcal{L}_{\text{Reblur}}^{\text{self}}$ to make the deblurred image even sharper. Figure 6 shows the test-time-adapted result with SRN. Compared with the baseline trained with L1 loss, our results exhibit improved trade-off relation between PSNR and the perceptual metrics, LPIPS and NIQE. Table 6 and 7 provide detailed quantitative test-time adaptation results on GOPRO and REDS dataset, respectively with various deblurring module architectures.

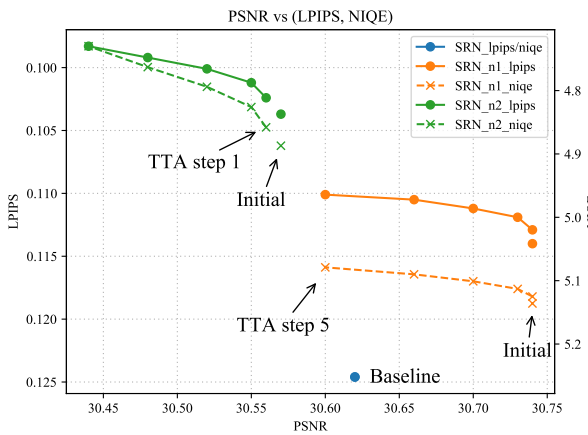


Figure 6: **Test-time adaption results using SRN on GO-PRO [27] dataset.** The proposed self-supervised objective improves trade-off between the perceptual image quality (LPIPS, NIQE) and PSNR compared with the baseline.

Method	LPIPS \downarrow	NIQE \downarrow	PSNR \uparrow	SSIM \uparrow
U-Net (\mathcal{L}_1)	0.1635	5.996	29.66	0.8874
U-Net ($\mathcal{L}_1 + \mathcal{L}_{\text{Reblur}, n1}$) + TTA step 5	0.1327	5.599	29.52	0.8878
U-Net ($\mathcal{L}_1 + \mathcal{L}_{\text{Reblur}, n2}$) + TTA step 5	0.1238	5.124	29.44	0.8824
SRN (\mathcal{L}_1)	0.1246	5.252	30.62	0.9078
SRN ($\mathcal{L}_1 + \mathcal{L}_{\text{Reblur}, n1}$) + TTA step 1	0.1140	5.136	30.74	0.9104
+ TTA step 3	0.1129	5.125	30.74	0.9107
+ TTA step 5	0.1112	5.101	30.70	0.9108
SRN ($\mathcal{L}_1 + \mathcal{L}_{\text{Reblur}, n2}$) + TTA step 5	0.1037	4.887	30.57	0.9074
DHN (\mathcal{L}_1)	0.1179	5.490	31.53	0.9207
DHN ($\mathcal{L}_1 + \mathcal{L}_{\text{Reblur}, n1}$) + TTA step 5	0.0975	5.472	31.53	0.9217
DHN ($\mathcal{L}_1 + \mathcal{L}_{\text{Reblur}, n2}$) + TTA step 5	0.0837	5.076	31.34	0.9177
SRN ($\mathcal{L}_1 + \mathcal{L}_{\text{Reblur}, n2}$) + TTA step 5	0.0983	4.730	30.44	0.9067

Table 6: **Test-time adaption results of various deblurring networks on GOPRO [27] dataset.**

4.5. Comparison with State-of-The-Art Methods

We have improved the perceptual quality of the deblurred images by training several different model architectures. We compare the perceptual quality with the other state-of-the-art methods in Figure 8. Especially, DeblurGAN-v2 was trained with the VGG loss and the adversarial loss. Our results achieve visually sharper texture from the reblurring loss and test-time adaptation.

4.6. Real World Image Deblurring

While our method uses synthetic datasets [27, 26] for training, the trained models generalize to real blurry im-

Method	LPIPS \downarrow	NIQE \downarrow	PSNR \uparrow	SSIM \uparrow
U-Net (\mathcal{L}_1)	0.1486	3.649	30.80	0.8772
U-Net ($\mathcal{L}_1 + \mathcal{L}_{\text{Reblur}, n2}$) + TTA step 5	0.1252	2.918	30.46	0.8717
SRN (\mathcal{L}_1)	0.1226	2.849	30.25	0.8701
SRN ($\mathcal{L}_1 + \mathcal{L}_{\text{Reblur}, n2}$) + TTA step 5	0.1148	3.392	31.89	0.8999
DHN (\mathcal{L}_1)	0.0942	3.288	32.65	0.9152
DHN ($\mathcal{L}_1 + \mathcal{L}_{\text{Reblur}, n2}$) + TTA step 5	0.0805	2.830	32.44	0.9122
SRN ($\mathcal{L}_1 + \mathcal{L}_{\text{Reblur}, n2}$) + TTA step 5	0.0763	2.761	32.17	0.9110

Table 7: **Test-time adaption results of various deblurring methods on REDS [26] dataset.**

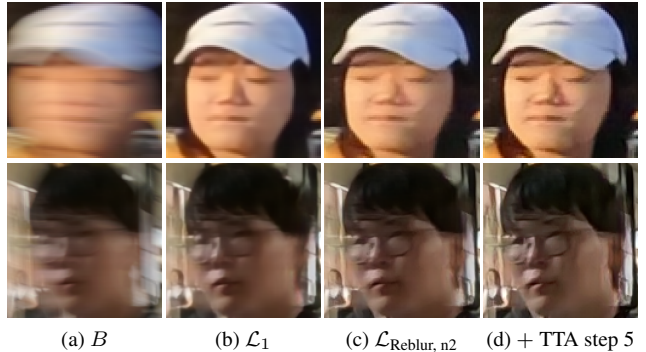


Figure 7: **Qualitative comparison between different training objectives and the test-time adaption.** Patches are sampled from the REDS [26] dataset validation split.

ages. In Figure 9, we show deblurred results from Lai *et al.* [19] dataset with DHN model. Compared with the baseline \mathcal{L}_1 loss, our reblurring loss $\mathcal{L}_{\text{Reblur}, n2}$ provides an improved deblurring quality. As the real test image could deviate from the training data distribution, a single forward inference may not produce optimal results. With the self-supervised test-time adaptation, our deblurred images reveal sharper and detailed textures.

5. Conclusion

In this paper, we validate a new observation that clean sharp images are hard to reblur and develop new low-level perceptual loss. We construct reblurring loss that cares for the image blurriness by jointly training a pair of deblurring and reblurring modules. The supervised reblurring loss provides an amplified view on motion blur while the self-supervised loss inspects the blurriness from the learned reblurring module weights. The self-supervision lets the deblurring module adapt to the new image at test time without ground truth. By applying the loss terms to the state-of-the-art deblurring architectures, we demonstrated our method consistently improves the the perceptual sharpness of the deblurred images both quantitatively and visually.

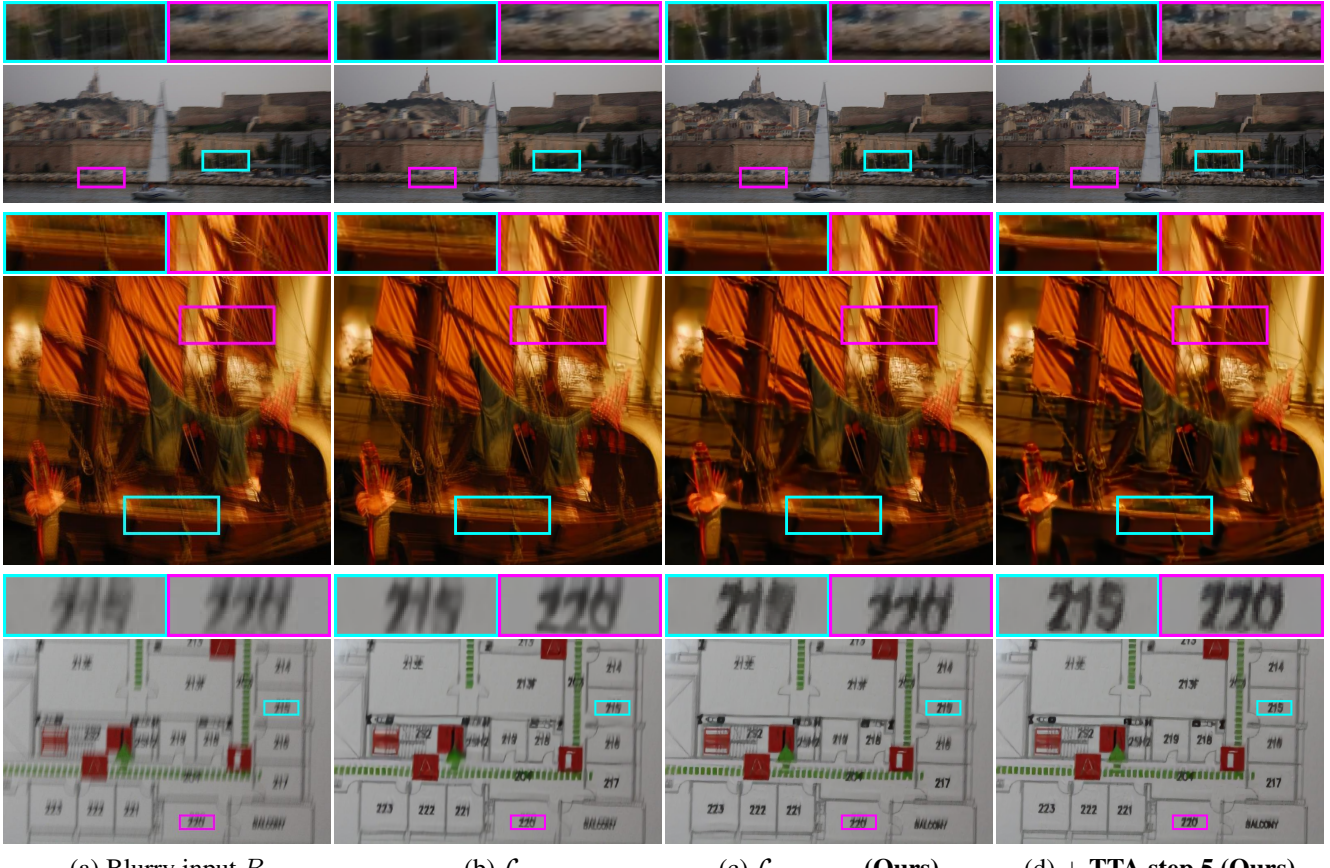
(a) Blurry input B

(b) SE-Sharing [8]

(c) DeblurGAN-v2 [18]

(d) Ours + TTA step 5

Figure 8: **Qualitative comparison between state-of-the-art deblurring methods on the GOPRO [27] dataset.** Our approach uses the SRN [43] model as a baseline architecture.

(a) Blurry input B (b) \mathcal{L}_1 (c) $\mathcal{L}_{\text{Reblur, n2}}$ (Ours)

(d) + TTA step 5 (Ours)

Figure 9: **Qualitative comparison of deblurring results on the real-world images [19] by different loss functions and test-time adaptation.** The proposed test-time adaptation greatly improves visual quality and sharpness of the deblurred images.

Appendix: Supplementary Material

In this supplementary material, we explain the detailed experimental results that are not shown in the main manuscript. In section S1, we show the implementation details with the model architecture specifics, training details, and the evaluation metrics. Section S2 describes how the reblurring module design and the size are determined. Then in section S3, we describe the different characteristics of the proposed reblurring loss and the other perceptual losses. We combine our reblurring loss with the other perceptual losses to take advantage in multiple perspectives. In section S4, we show the effect of test-time adaptation and show the trade-off relation between the conventional distortion quality metric (PSNR, SSIM) and the perceptual metrics (LPIPS, NIQE) compared with the baselines. In section S5, we visually validate the effect of reblurring loss and test-time adaptation.

S1. Implementation Details

Model Architecture. In the main manuscript, we performed the experiments with 3 model architectures. We set our baseline model as a light-weight residual U-Net architecture that runs in fast speed. The baseline model is used to design our reblurring loss with pseudo-sharp images through ablation study in Table 4.

For reblurring operation, we use a simple residual network \mathcal{M}_R without strides to avoid deconvolution artifacts. The baseline U-Net and the reblurring module architectures are shown in Figure S1. The detailed parameters for U-Net and \mathcal{M}_R are each specified in Table S1 and S3.

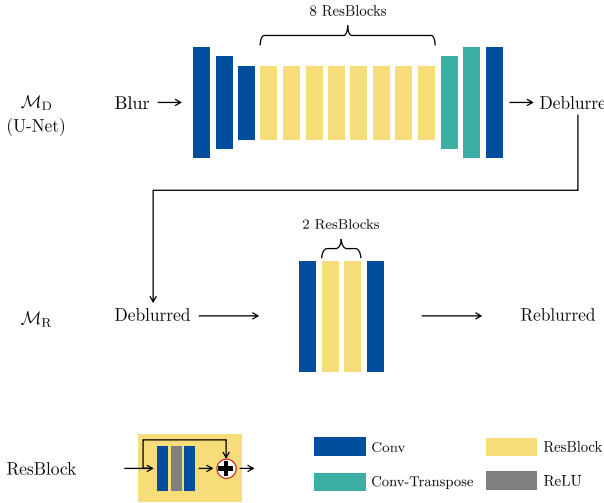


Figure S1: The baseline U-Net architecture and the reblurring module architecture We use the same reblurring module for all experiments except the number of Res-Blocks.

#	Layer description	Output shape
	Input	$3 \times H \times W$
1	5×5 conv	$64 \times H \times W$
2	3×3 conv	$128 \times H/2 \times W/2$
3	3×3 conv	$192 \times H/4 \times W/4$
4-19	8 ResBlocks (3×3)	$192 \times H/4 \times W/4$
20	3×3 conv	$128 \times H/2 \times W/2$
21	3×3 conv	$64 \times H \times W$
22	5×5 conv	$3 \times H \times W$

Table S1: U-Net module specifics

Method	LPIPS \downarrow	NIQE \downarrow	PSNR \uparrow	SSIM \uparrow
DMPHN (\mathcal{L}_1 only)	0.1184	5.542	31.42	0.9191
DHN (\mathcal{L}_1 only)	0.1179	5.490	31.53	0.9207

Table S2: **DMPHN modification results on GOPRO [27] dataset.** DHN without patch-wise convolution brings improved accuracy.

In addition to the U-Net, experiments were conducted with state-of-the-art deblurring models based on SRN [42] and DMPhN [49]. SRN [43] was originally designed to operate on grayscale images with a LSTM module. Later, the authors released the sRGB version code without LSTM, exhibiting an improved accuracy. We adopted the revised SRN structure in our experiments.

The other model we chose is based on DMPhN (1-2-4-8) [49]. DMPhN performs hierarchical residual refinement to produce the final output. The model consists of convolutional layers with ReLU activations that are spatially shift-equivariant. In [49], each level splits the given image and performs the convolutional operation on the divided patches. As the convolutional weights do not differ by the patches, the operations do not necessarily have to be done patch-wise. Thus, we remove the multi-patch strategy and perform the convolution on the whole given input without dividing the image into patches. We refer to the modified model as DHN. As shown in Table S2, convolution on the whole image compared with patch-wise convolution brings higher accuracy.

Metrics To quantitatively compare the deblurred images in the following sections, we use PSNR, SSIM [45], LPIPS [52], and NIQE [25]. In the image deblurring literature, SSIM has been measured by MATLAB `ssim` function on sRGB images with $H \times W \times C$. SSIM was originally developed for grayscale images and MATLAB `ssim` function for a 3-dimensional tensor considers an image to be a 3D grayscale volume image. Thus, most of the previous SSIM measures were not accurate, leading to higher values. Instead, we measured all the SSIM for each channel separately and averaged them. We used `skimage.metrics.structural_similarity` function in the scikit-image package for python to measure SSIM for multi-channel images.

#	Layer description	Output shape
	Input	$3 \times H \times W$
1	5×5 conv	$64 \times H \times W$
2-5	2 ResBlocks (5×5)	$64 \times H/4 \times W/4$
6	5×5 conv	$3 \times H \times W$

Table S3: Reblurring module specifics

Training For all the experiments, we performed the same training process for a fair comparison. On the GOPRO dataset [27], we trained each model for 4000 epochs. On the REDS dataset [26], the models are trained for 200 epochs. Adam [16] optimizer is used in all cases. When calculating distance between images with Lp norm, we always set $p = 1$, using L1 distance. Starting from the initial learning rate 1×10^{-4} , the learning rate halves when training reaches 50%, 75%, and 90% of the total epochs. We used PyTorch 1.7.1 with CUDA 11.0 to implement the deblurring methods. Mixed-precision training [24] is employed to accelerate operations on RTX 2080 Ti GPUs.

S2. Determining Reblurring Module Size

As our reblurring loss \mathcal{L}_R is realized by \mathcal{M}_R , the reblurring module design plays an essential role. As shown in Figure S1, the \mathcal{M}_R architecture is a simple ResNet. Table S4 shows the relation between the deblurring performance and \mathcal{M}_R size by changing the number of ResBlocks.

For all deblurring module \mathcal{M}_D architectures, LPIPS was the best when the number of ResBlocks, $n = 2$. NIQE showed good performance when $2 \leq n \leq 3$. PSNR and SSIM had tendency to decrease when $n \geq 1$. For larger number of ResBlocks, we witnessed sharper edges could be obtained but sometimes, cartoon artifacts with over-strong edges were witnessed.

Considering the trade-off between the PSNR and the perceptual metrics, we chose $n \in \{1, 2\}$ in the following experiments. $n = 1$ finds balance between the PSNR and LPIPS and $n = 2$ puts more weight on the perceptual quality.

S3. Combining Reblurring Loss with Other Perceptual Losses

Our reblurring loss is a new perceptual loss that is sensitive to blurriness of an image, a type of image structure-level information while other perceptual losses such as VGG loss [13] and adversarial loss [20] are more related to the high-level contexts. As VGG model [37] is trained to recognize image classes, optimizing with VGG loss could make an image better recognizable. In the GAN frameworks [10], it is well known that discriminators can easily tell fake images from real images [44], being robust against JPEG compression and blurring. In the adversarial loss from the discriminator, the realism difference could be more salient than other features such as blurriness.

Method	LPIPS \downarrow	NIQE \downarrow	PSNR \uparrow	SSIM \uparrow
U-Net (\mathcal{L}_1 only)	0.1635	5.996	29.66	0.8874
$+\mathcal{L}_{\text{Reblur, n1}}$	0.1365	5.629	29.58	0.8869
$+\mathcal{L}_{\text{Reblur, n2}}$	0.1238	5.124	29.44	0.8824
$+\mathcal{L}_{\text{Reblur, n3}}$	0.1386	5.448	29.38	0.8819
$+\mathcal{L}_{\text{Reblur, n4}}$	0.1415	5.513	29.25	0.8789
SRN (\mathcal{L}_1 only)	0.1246	5.252	30.62	0.9078
$+\mathcal{L}_{\text{Reblur, n1}}$	0.1140	5.136	30.74	0.9104
$+\mathcal{L}_{\text{Reblur, n2}}$	0.1037	4.887	30.57	0.9074
$+\mathcal{L}_{\text{Reblur, n3}}$	0.1091	4.875	30.50	0.9060
$+\mathcal{L}_{\text{Reblur, n4}}$	0.1155	5.041	30.53	0.9056
DHN (\mathcal{L}_1 only)	0.1179	5.490	31.53	0.9207
$+\mathcal{L}_{\text{Reblur, n1}}$	0.0975	5.472	31.53	0.9217
$+\mathcal{L}_{\text{Reblur, n2}}$	0.0837	5.076	31.34	0.9177
$+\mathcal{L}_{\text{Reblur, n3}}$	0.0845	4.963	31.26	0.9159
$+\mathcal{L}_{\text{Reblur, n4}}$	0.0861	5.041	31.19	0.9149

Table S4: The effect of reblurring loss on GOPRO [27] dataset by the reblurring module size. Reblurring module size varies by the number of ResBlocks.

Method	LPIPS \downarrow	NIQE \downarrow	PSNR \uparrow	SSIM \uparrow
SRN (\mathcal{L}_1 only)	0.1246	5.252	30.62	0.9078
$+\mathcal{L}_{\text{VGG}}$	0.1037	4.945	30.60	0.9074
$+\mathcal{L}_{\text{VGG}} + \mathcal{L}_{\text{Reblur, n2}}$	0.0928	4.671	30.64	0.9079
$+\mathcal{L}_{\text{Adv}}$	0.1141	4.960	30.53	0.9068
$+\mathcal{L}_{\text{Adv}} + \mathcal{L}_{\text{Reblur, n2}}$	0.1014	4.811	30.56	0.9075
DHN (\mathcal{L}_1 only)	0.1179	5.490	31.53	0.9207
$+\mathcal{L}_{\text{VGG}}$	0.0994	5.022	31.48	0.9195
$+\mathcal{L}_{\text{VGG}} + \mathcal{L}_{\text{Reblur, n2}}$	0.0773	4.897	31.28	0.9161
$+\mathcal{L}_{\text{Adv}}$	0.0969	5.026	31.46	0.9188
$+\mathcal{L}_{\text{Adv}} + \mathcal{L}_{\text{Reblur, n2}}$	0.0835	4.799	31.28	0.9162

Table S5: Results on GOPRO [27] dataset by adding reblurring loss to the other perceptual losses.

Method	LPIPS \downarrow	NIQE \downarrow	PSNR \uparrow	SSIM \uparrow
SRN (\mathcal{L}_1 only)	0.1148	3.392	31.89	0.8999
$+\mathcal{L}_{\text{VGG}}$	0.1000	3.256	31.86	0.9001
$+\mathcal{L}_{\text{VGG}} + \mathcal{L}_{\text{Reblur, n2}}$	0.0868	2.835	31.83	0.9015
DHN (\mathcal{L}_1 only)	0.0942	3.288	32.65	0.9152
$+\mathcal{L}_{\text{VGG}}$	0.0812	3.171	32.61	0.9146
$+\mathcal{L}_{\text{VGG}} + \mathcal{L}_{\text{Reblur, n2}}$	0.0723	2.821	32.48	0.9133

Table S6: Results on REDS [26] dataset by adding reblurring loss to the other perceptual losses.

With the perceptual loss functions designed with different objectives, combining them could bring visual quality improvements in various aspects. Table S5 and S5 shows the effect of applying our reblurring loss jointly with the other perceptual losses on GOPRO and REDS datasets. We omit the loss coefficients for simplicity. We used weight 0.3 for the VGG loss \mathcal{L}_{VGG} and 0.001 for the adversarial loss, \mathcal{L}_{Adv} . We witness LPIPS and NIQE further improves when our reblurring loss is combined with \mathcal{L}_{VGG} or \mathcal{L}_{Adv} .

S4. Perception vs. Distortion Trade-Off

It is known in image restoration literature that the distortion error and the perceptual quality error are in trade-off relation [4, 3]. The relation is often witnessed by training a single model with different loss functions. In most cases, to obtain a better perceptual quality from a single model architecture, retraining with another loss from scratch is necessary. Our test-time adaptation from self-supervised reblurring loss, in contrast, can provide the steps toward perceptual quality without full retraining.

In Figure S2 and S3, we present the perception-distortion trade-off from our test-time adaption. LPIPS and NIQE scores consistently improve from each adaptation step in both SRN and DHN models. While PSNR is moderately sacrificed from the adaptation, SSIM improves in the early steps as it more reflects the structural information. Our results show improved trade-off between the distortion and perception metrics over the baseline models trained with L1 loss. d trade-off between the distortion and perception metrics over the baseline trained with L1 loss.

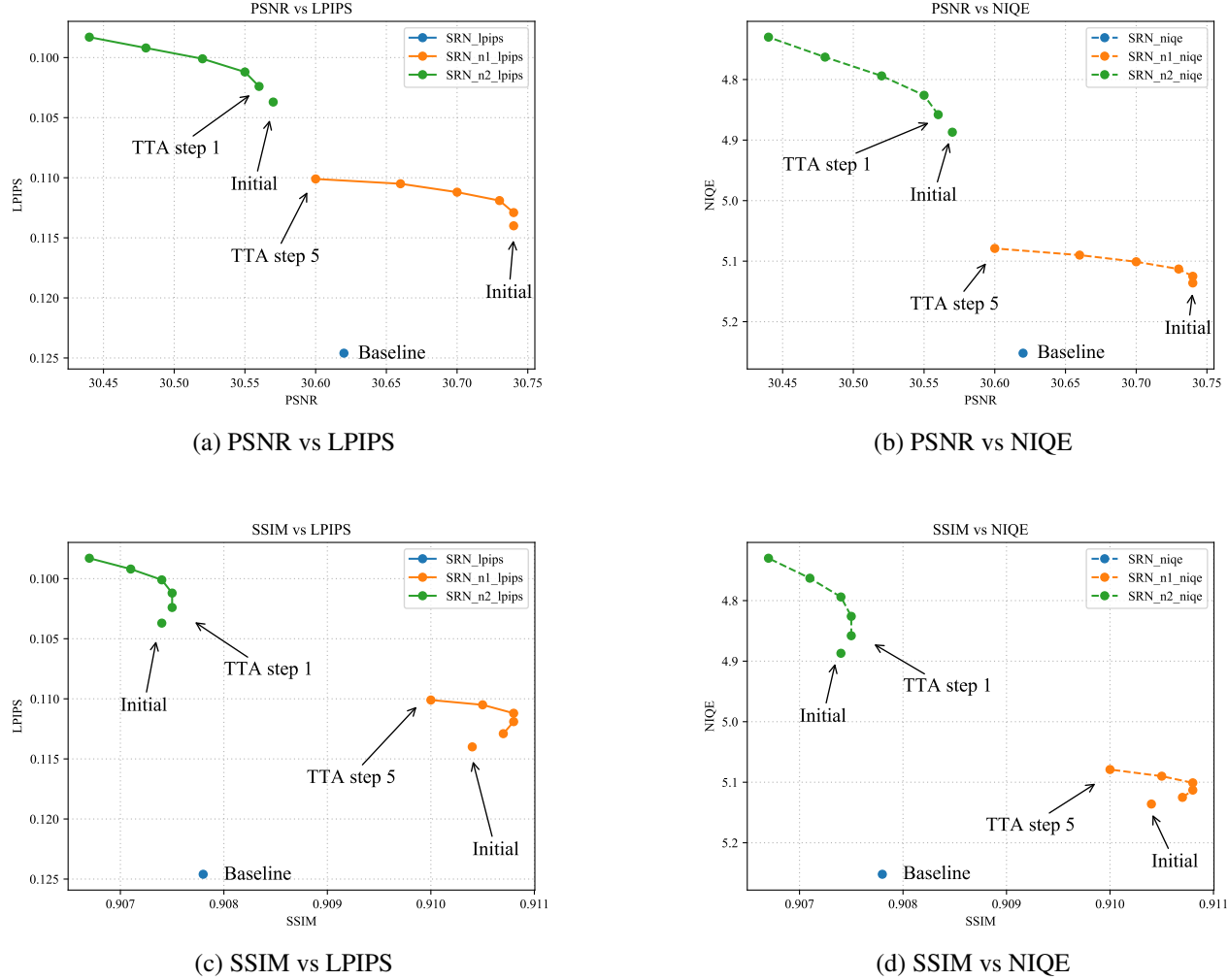


Figure S2: Perception-distortion trade-off from test-time adaptation applied to SRN model on GOPRO [27] dataset.

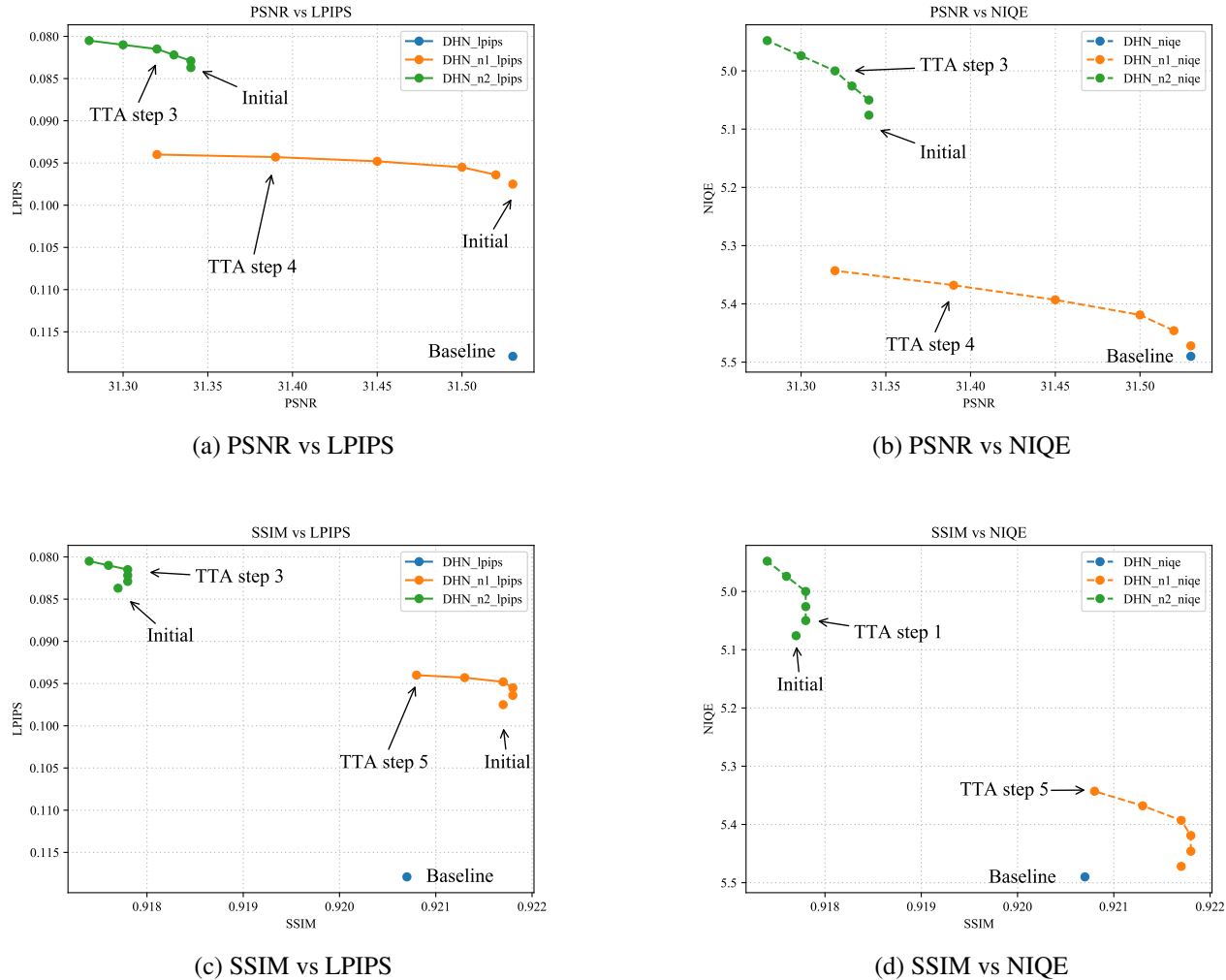


Figure S3: Perception-distortion trade-off from test-time adaptation applied to DHN model on GOPRO [27] dataset.

S5. Visual Comparison of Loss Function

In this section, we present the visual comparison of deblurred results. In Figure S4 and S5, we perform visual ablation by showing the deblurred results from baseline L1 loss, our reblurring loss, and additional test-time adaptation. For \mathcal{M}_D , we used DHN. For \mathcal{M}_R , 2 ResBlocks are used. Our final result reveals sharper image structure and texture.

In Figure S6 and S7, we compare the effect of 3 different perceptual losses. The results from VGG loss, adversarial loss, and our reblurring loss are shown. Our reblurring loss exhibits clearer edges and the face details than other perceptual losses.



(a) Blur

(b) Our deblurred image (TTA step 5)



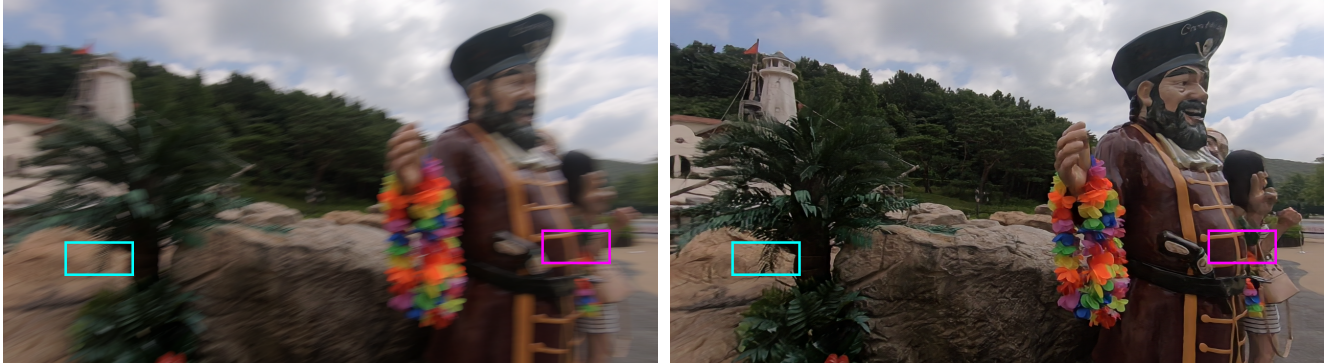
(c) Blur B

(d) \mathcal{L}_1

(e) $\mathcal{L}_1 + \mathcal{L}_{\text{Reblur}, n2}$

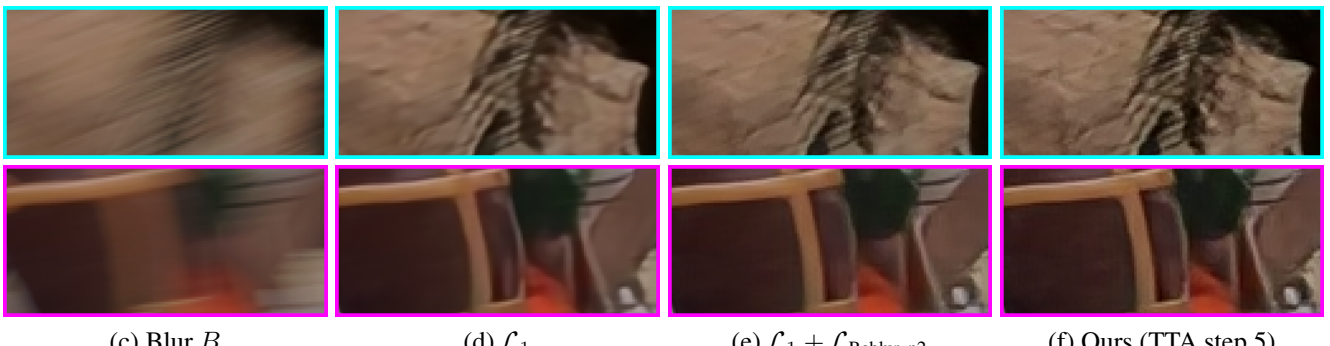
(f) Ours (TTA step 5)

Figure S4: Visual comparison of deblurred results by reblurring loss and test-time adaptation on REDS [26] dataset.



(a) Blur

(b) Our deblurred image (TTA step 5)



(c) Blur B

(d) \mathcal{L}_1

(e) $\mathcal{L}_1 + \mathcal{L}_{\text{Reblur}, n2}$

(f) Ours (TTA step 5)

Figure S5: Visual comparison of deblurred results by reblurring loss and test-time adaptation on REDS [26] dataset.



(a) Blur

(b) Our deblurred image ($\mathcal{L}_1 + \mathcal{L}_{\text{Reblur, n2}}$)(c) Blur B (d) \mathcal{L}_1 (e) $\mathcal{L}_1 + \mathcal{L}_{\text{VGG}}$ (f) $\mathcal{L}_1 + \mathcal{L}_{\text{Adv}}$ (g) $\mathcal{L}_1 + \mathcal{L}_{\text{Reblur, n2}}$

Figure S6: Visual comparison of perceptual losses on REDS [26] dataset.



(a) Blur

(b) Our deblurred image ($\mathcal{L}_1 + \mathcal{L}_{\text{Reblur, n2}}$)(c) Blur B (d) \mathcal{L}_1 (e) $\mathcal{L}_1 + \mathcal{L}_{\text{VGG}}$ (f) $\mathcal{L}_1 + \mathcal{L}_{\text{Adv}}$ (g) $\mathcal{L}_1 + \mathcal{L}_{\text{Reblur, n2}}$

Figure S7: Visual comparison of perceptual losses on REDS [26] dataset.

References

[1] Soonmin Bae and Frédo Durand. Defocus magnification. *Computer Graphics Forum*, 26(3):571–579, 2007. 3

[2] Yuval Bahat, Netalee Efrat, and Michal Irani. Non-uniform blind deblurring by reblurring. In *ICCV*, 2017. 3

[3] Yochai Blau, Roey Mechrez, Radu Timofte, Tomer Michaeli, and Lihai Zelnik-Manor. The 2018 pirm challenge on perceptual image super-resolution. In *Proceedings of the ECCV Workshops*, September 2018. 11

[4] Yochai Blau and Tomer Michaeli. The perception-distortion tradeoff. In *CVPR*, 2018. 11

[5] Tim Brooks and Jonathan T. Barron. Learning to synthesize motion blur. In *CVPR*, 2019. 3

[6] Huaijin Chen, Jinwei Gu, Orazio Gallo, Ming-Yu Liu, Ashok Veeraraghavan, and Jan Kautz. Reblur2deblur: Deblurring videos via self-supervised learning. In *ICCP*, 2018. 3

[7] Sunghyun Cho and Seungyong Lee. Fast motion deblurring. In *ACM SIGGRAPH Asia*, 2009. 1, 2

[8] Hongyun Gao, Xin Tao, Xiaoyong Shen, and Jiaya Jia. Dynamic scene deblurring with parameter selective sharing and nested skip connections. In *CVPR*, 2019. 1, 2, 8

[9] Dong Gong, Jie Yang, Lingqiao Liu, Yanning Zhang, Ian Reid, Chunhua Shen, Anton van den Hengel, and Qinfeng Shi. From motion blur to motion flow: A deep learning solution for removing heterogeneous motion blur. In *CVPR*, 2017. 2

[10] Ian Goodfellow, Jean Pouget-Abadie, Mehdi Mirza, Bing Xu, David Warde-Farley, Sherjil Ozair, Aaron Courville, and Yoshua Bengio. Generative adversarial nets. In *NIPS*, 2014. 2, 3, 4, 10

[11] Michael Hirsch, Christian J Schuler, Stefan Harmeling, and Bernhard Schölkopf. Fast removal of non-uniform camera shake. In *ICCV*, 2011. 1, 2

[12] Meiguang Jin, Zhe Hu, and Paolo Favaro. Learning to extract flawless slow motion from blurry videos. In *CVPR*, 2019. 2

[13] Justin Johnson, Alexandre Alahi, and Li Fei-Fei. Perceptual losses for real-time style transfer and super-resolution. In *ECCV*, 2016. 1, 2, 3, 6, 10

[14] Tae Hyun Kim, Byeongjoo Ahn, and Kyoung Mu Lee. Dynamic scene deblurring. In *ICCV*, 2013. 1, 2

[15] Tae Hyun Kim and Kyoung Mu Lee. Segmentation-free dynamic scene deblurring. In *CVPR*, 2014. 1, 2

[16] Diederik P Kingma and Jimmy Ba. Adam: A method for stochastic optimization. *arXiv preprint arXiv:1412.6980*, 2014. 10

[17] Orest Kupyn, Volodymyr Budzan, Mykola Mykhailych, Dmytro Mishkin, and Jiří Matas. DeblurGAN: Blind motion deblurring using conditional adversarial networks. In *CVPR*, 2018. 1, 3

[18] Orest Kupyn, Tetiana Martyniuk, Junru Wu, and Zhangyang Wang. DeblurGAN-v2: Deblurring (orders-of-magnitude) faster and better. In *ICCV*, 2019. 2, 3, 8

[19] Wei-Sheng Lai, Jia-Bin Huang, Zhe Hu, Narendra Ahuja, and Ming-Hsuan Yang. A comparative study for single image blind deblurring. In *CVPR*, 2016. 7, 8

[20] Christian Ledig, Lucas Theis, Ferenc Huszar, Jose Caballero, Andrew Cunningham, Alejandro Acosta, Andrew Aitken, Alykhan Tejani, Johannes Totz, Zehan Wang, and Wenzhe Shi. Photo-realistic single image super-resolution using a generative adversarial network. In *CVPR*, 2017. 1, 3, 10

[21] Anat Levin. Blind motion deblurring using image statistics. *NIPS*, 2006. 2

[22] Lerenhan Li, Jinshan Pan, Wei-Sheng Lai, Changxin Gao, Nong Sang, and Ming-Hsuan Yang. Learning a discriminative prior for blind image deblurring. In *CVPR*, 2018. 2

[23] Sachit Menon, Alexandru Damian, Shijia Hu, Nikhil Ravi, and Cynthia Rudin. PULSE: Self-supervised photo upsampling via latent space exploration of generative models. In *CVPR*, 2020. 1, 2

[24] Paulius Micikevicius, Sharan Narang, Jonah Alben, Gregory Diamos, Erich Elsen, David Garcia, Boris Ginsburg, Michael Houston, Oleksii Kuchaiev, Ganesh Venkatesh, et al. Mixed precision training. *arXiv preprint arXiv:1710.03740*, 2017. 10

[25] Anish Mittal, Rajiv Soundararajan, and Alan C Bovik. Making a “completely blind” image quality analyzer. *IEEE SPL*, 20(3):209–212, 2012. 5, 9

[26] Seungjun Nah, Sungyong Baik, Seokil Hong, Gyeongsik Moon, Sanghyun Son, Radu Timofte, and Kyoung Mu Lee. NTIRE 2019 challenges on video deblurring and super-resolution: Dataset and study. In *CVPR Workshops*, 2019. 1, 2, 5, 7, 10, 14, 15

[27] Seungjun Nah, Tae Hyun Kim, and Kyoung Mu Lee. Deep multi-scale convolutional neural network for dynamic scene deblurring. In *CVPR*, 2017. 1, 2, 3, 5, 6, 7, 8, 9, 10, 11, 12

[28] Yuesong Nan and Hui Ji. Deep learning for handling kernel/model uncertainty in image deconvolution. In *CVPR*, 2020. 2

[29] T. M. Nimisha, Akash Kumar Singh, and A. N. Rajagopalan. Blur-invariant deep learning for blind-deblurring. In *ICCV*, 2017. 3

[30] Mehdi Noroozi, Paramanand Chandramouli, and Paolo Favaro. Motion deblurring in the wild. In *GCPR*, 2017. 1, 2

[31] Jinshan Pan, Deqing Sun, Hanspeter Pfister, and Ming-Hsuan Yang. Blind image deblurring using dark channel prior. In *CVPR*, 2016. 2

[32] Dongwon Park, Dong Un Kang, Jisoo Kim, and Se Young Chun. Multi-temporal recurrent neural networks for progressive non-uniform single image deblurring with incremental temporal training. In *ECCV*, 2020. 1, 2

[33] Dongwei Ren, Kai Zhang, Qilong Wang, Qinghua Hu, and Wangmeng Zuo. Neural blind deconvolution using deep priors. In *CVPR*, 2020. 2

[34] Olga Russakovsky, Jia Deng, Hao Su, Jonathan Krause, Sanjeev Satheesh, Sean Ma, Zhiheng Huang, Andrej Karpathy, Aditya Khosla, Michael Bernstein, et al. ImageNet large scale visual recognition challenge. *IJCV*, 115(3):211–252, 2015. 3

[35] Christian J Schuler, Michael Hirsch, Stefan Harmeling, and Bernhard Schölkopf. Learning to deblur. *IEEE TPAMI*, 38(7):1439–1451, 2015. 2

[36] Ziyi Shen, Wenguan Wang, Xiankai Lu, Jianbing Shen, Haibin Ling, Tingfa Xu, and Ling Shao. Human-aware motion deblurring. In *ICCV*, 2019. 1, 2

[37] Karen Simonyan and Andrew Zisserman. Very deep convolutional networks for large-scale image recognition. *arXiv preprint arXiv:1409.1556*, 2014. 3, 10

[38] Shuochen Su, Mauricio Delbracio, Jue Wang, Guillermo Sapiro, Wolfgang Heidrich, and Oliver Wang. Deep video deblurring for hand-held cameras. In *CVPR*, 2017. 1, 2

[39] Maitreya Suin, Kuldeep Purohit, and A. N. Rajagopalan. Spatially-attentive patch-hierarchical network for adaptive motion deblurring. In *CVPR*, 2020. 2

[40] Jian Sun, Wenfei Cao, Zongben Xu, and Jean Ponce. Learning a convolutional neural network for non-uniform motion blur removal. In *CVPR*, 2015. 2

[41] Libin Sun, SungHyun Cho, Jue Wang, and James Hays. Edge-based blur kernel estimation using patch priors. In *ICCP*, 2013. 2

[42] Xin Tao, Hongyun Gao, Renjie Liao, Jue Wang, and Jiaya Jia. Detail-revealing deep video super-resolution. In *ICCV*, 2017. 1, 9

[43] Xin Tao, Hongyun Gao, Xiaoyong Shen, Jue Wang, and Jiaya Jia. Scale-recurrent network for deep image deblurring. In *CVPR*, 2018. 2, 5, 6, 8, 9

[44] Sheng-Yu Wang, Oliver Wang, Richard Zhang, Andrew Owens, and Alexei A. Efros. CNN-Generated images are surprisingly easy to spot... for now. In *CVPR*, 2020. 4, 10

[45] Zhou Wang, Alan C Bovik, Hamid R Sheikh, Eero P Simoncelli, et al. Image quality assessment: from error visibility to structural similarity. *IEEE TIP*, 13(4):600–612, 2004. 9

[46] Oliver Whyte, Josef Sivic, Andrew Zisserman, and Jean Ponce. Non-uniform deblurring for shaken images. *IJCV*, 98(2):168–186, 2012. 1, 2

[47] Li Xu, Shicheng Zheng, and Jiaya Jia. Unnatural L0 sparse representation for natural image deblurring. In *CVPR*, 2013. 2

[48] Yuan Yuan, Wei Su, and Dandan Ma. Efficient dynamic scene deblurring using spatially variant deconvolution network with optical flow guided training. In *CVPR*, 2020. 1, 2

[49] Hongguang Zhang, Yuchao Dai, Hongdong Li, and Piotr Koniusz. Deep stacked hierarchical multi-patch network for image deblurring. In *CVPR*, 2019. 2, 5, 9

[50] Jiawei Zhang, Jinshan Pan, Jimmy Ren, Yibing Song, Linchao Bao, Rynson W.H. Lau, and Ming-Hsuan Yang. Dynamic scene deblurring using spatially variant recurrent neural networks. In *CVPR*, 2018. 2

[51] Kaihao Zhang, Wenhan Luo, Yiran Zhong, Lin Ma, Bjorn Stenger, Wei Liu, and Hongdong Li. Deblurring by realistic blurring. In *CVPR*, 2020. 3

[52] Richard Zhang, Phillip Isola, Alexei A. Efros, Eli Shechtman, and Oliver Wang. The unreasonable effectiveness of deep features as a perceptual metric. In *CVPR*, 2018. 2, 3, 5, 9